Supplementary Information (SI) for Nanoscale.
This journal is © The Royal Society of Chemistry 2026

Supporting Information

Engineering CNT-supported PtRu nanoparticles with ultrathin carbon coating for optimized d-Band center and superior methanol oxidation performance

Xin Wang, [a] Zhongqing Jiang, [b] Binglu Deng [c] and Zhong-Jie Jiang [*a]

[a] *Guangzhou Key Laboratory for Surface Chemistry of Energy Materials, Guangdong Engineering and Technology Research Center for Surface Chemistry of Energy Materials, New Energy Research Institute, College of Environment and Energy, South China University of Technology, Guangzhou 510006, P. R. China. E-mail: eszjiang@scut.edu.cn*

[b] *Key Laboratory of Optical Field Manipulation of Zhejiang Province, Depa rtment of Physics, Zhejiang Sci-Tech University, Hangzhou 310018, P. R. China.*

[c] *School of Materials Science and Hydrogen Energy, Foshan University, Foshan 52800, P. R. China.*

1. Experimental section

1.1. Reagants

All chemical reagents were used as received without further purification. Carbon nanotubes (CNTs) with diameter of 40-60 nm and length of 5-15 μm, (amorphous carbon content <3%) were obtained from Shenzhen Nanotech Port Co. Ltd. Chloroplatinic acid hydrate ($H_2PtCl_6 \cdot 6H_2O$, Pt≥37.5%), ruthenium(III) chloride hydrate ($RuCl_3 \cdot xH_2O$, Ru≥37%), and aniline (95%) were purchased from Shanghai Macklin Biochemical Ltd. Ammonium peroxodisulfate (APS, 98%) and hexamethylenetetramine (98.0%) were bought from Tianjin Damao Chemical Reagent Co. Ltd. Concentrated mineral acids (HNO_3, ≥68%; H_2SO_4, 98%) were acquired from Guangzhou Chemical Reagents Co. Commercial Pt/C catalyst (20 wt.% Pt) and Nafion solution (5.0 wt.% in isopropanol) were obtained from Shanghai Aladdin Bio-Chem Technology Co. Ltd. and Dupont China Holding Ltd., respectively. Ultrapure water with the resistence of 18.2 MΩ cm^{-1} was ultized in all the experiments.

1.2. Synthesis of PtRu/CNTs

The acid-treated CNTs were used for the synthesis of the PtRu/CNTs. Specifically, the CNTs were dispersed in a mixed HNO_3/H_2SO_4 solution (V_{HNO_3} : $V_{H_2SO_4}$ = 1:1) and refluxed at 80 °C for 4 h. The The acid treating made the CNTs hydrophilic and readily dispersible in aqueous solutions for the subsequent use for the synthesis of the PtRu/CNTs. After thorough washing with deionized (DI) water, the acid-treated CNTs were dispersed in DI water.

For the preparation of PtRu/CNTs, 3.0 mL of acid-treated CNTs aqueous solution (5.0 mg mL^{-1}) was ultrasonically dispersed in 24.0 mL of DI water. 1.0 mL of H_2PtCl_6 (0.03 mmol mL^{-1}) and 1.0 mL of $RuCl_3$ (0.03 mmol mL^{-1}) were sequentially added. After 0.5 h of ultrosonication, 1.0 mL of hexamethylenetetramine (50.0 mg mL^{-1}) was introduced under vigorous stirring. The resulting precursor was stirred for 0.5 h and then transferred to a 50 mL autoclave for the hyrdothermal reaction at 180 °C for 4 h. The obtained PtRu/CNTs were centrifuged and washed with anhydrous ethanol ≥ 3 times and then dried at 60 °C.

1.3. Synthesis of CN@PtRu/CNTs

20.0 mg of the PtRu/CNTs synthesized above was dispersed in 20.0 mL of DI water. The reaction mixture was cooled in an ice-water bath, followed by the sequential addition of two solutions: (1) 5.0 mL of 0.5 M HCl containing 60.0 mg ammonium peroxodisulfate (APS) and (2) 5.0 mL of 0.5 M HCl containing 30.0 μL aniline. The reaction was lasted for ~10 h. The resulting PANI@PtRu/CNTs were collected by centrifugation, washed thoroughly with ethanol (>3 times), and calcined at 325 ^oC in a tube furnace under air atmosphere, yielding the final product of CN@PtRu/CNTs.

For comparison, the PANI@PtRu/CNTs were also calcined at the different temperatures (300, 350, and 400 ^oC) to produce CN@PtRu/CNTs-300, CN@PtRu/CNTs-350, and PtRu/CNTs-400, respectively. To acquire the CN@PtRu/CNTs with optimal MOR catalytic activity, we prepared a series of the PANI@PtRu/CNTs by keeping the dosage of the H_2PtCl_6 solution (1.0 mL, 0.03 mmol mL-1) unchanged and adjusting the volume of the $RuCl_3$ solution (0.03 mmol mL^{-1}),

then thermally calcined at 325 °C. The experimental results confirm that the catalyst prepared using 1.0 mL H_2PtCl_6 and 1.0 mL $RuCl_3$ solutions exhibit the optimal MOR activity, and its actual Pt-to-Ru atomic ratio was determined to be 1.74:1.00 (**Figure S12**).

1.4. Characterization

An X-ray diffractometer (XRD, Bruker D8 Advance, Germany) using Cu Kα radiation (λ = 1.5406 Å) was utilized to determin the crystalline nature of the samples.X-ray photoelectron spectra (XPS) were recorded on a Thermo Fisher Nexsa spectrometer (USA) with Al Kα excitation (12 kV). The XPS spectra reported in this work were calibrated using C 1s at 248.6 eV. Morphological characterizations were conducted using a JEOL-JEM 2100F transmission electron microscope (TEM, Japan) operated at 200 kV, equipped with an energy-dispersive X-ray spectrometer (EDX). Elemental compositions was quantified by an inductively coupled plasma optical emission spectrometer (ICP-OES, Thermo Fisher iCAP 7200 Duo, USA).

1.5. Electrochemical measurements

A CHI 760E workstation using a standard three-electrode cell was utilized to evaluate the MOR activities of the samples. A carbon rod served as the counter electrode. Hg/Hg_2SO_4 was employed as the reference electrode in the acidic (0.5 M Hg_2SO_4 + 1 M CH_3OH) media. The catalyst ink was prepared by dispersing the catalyst (4.0 mg) in 1.0 mL of isopropanol containing 20.0 μL of the Nafion solution by ultrasonication. The catalyst loaded glassy carbon (GC, 5.0 mm in diameter) was used

as the working electrode. Before use, the GC electrode was polished with 0.05 μm Al_2O_3 powder and thoroughly rinsed with water. The working electrode was prepared by drop-casting the catalyst ink onto the GC electrode and drying naturally. The catalyst mass loading was controlled to be ~0.2 mg cm^{-2}. Cyclic voltammetries (CVs) were recorded at a scan rate of 50.0 mV s^{-1}. The CVs reported in this work were calibrated against the reversible hydrogen electrode (RHE). The chronoamperometric response was recorded at a constant potential of 0.7 V vs. RHE to evaluate the long-term stability and poisoning resistance of the catalyst. Electrochemical impedance spectra (EISs) were obtained within the frequency range of 10^5 Hz to 10^{-2} Hz.

The electrochemical surface area (ECSA) was evaluated from the CV between +0.05 and +0.40 V.

$$\text{ECSA} = Q/\Gamma m \qquad \text{(S1)}$$

where Q, Γ and m represent the transferred charge, the specific charge (210 μC cm^{-2}) of a hydrogen monolayer on a polycrystalline Pt surface, and the mass of Pt on the GCE, respectively.

Tafel slopes were derived from the positive-going scans of the MOR polarization curves (ECSA-normalized current density) within the low overpotential region (kinetically controlled region, approximately 0.40–0.65 V vs. RHE), where the plot of overpotential (η) vs. log(j) exhibits a linear relationship. The equilibrium potential for MOR was taken as 0.20 V vs. RHE. The slopes were obtained by linear fitting of the η–log(j) plots.

The CO stripping experiments were performed in 0.5 M H_2SO_4. Initially, the CO adsorption was carried out by maintaining the working electrode potential at 0.3 V vs. RHE under the CO bubbling for >30 min. The dissolved CO was then purged from the electrolyte through the N_2 bubbling for 30 min. The stripping voltammograms were recorded by scanning the potential anodically from 0.3 V vs. RHE at 20.0 mV s^{-1}. Att least two consecutive cycles were collected to ensure the reproducibility.

1.6. Evaluatioin of DFMCs

For evaluation of the applicability of the CN@PtRu/CNTs in the DMFCs, a membrane electrode assembly was prepared. Specifically, the CN@PtRu/CNTs and the commercial Pt/C (20.0 wt. %) were used as the anode (MOR) and cathode (oxygen reduction reaction, ORR) catalysts, respectively. Nafion 115 was used as the proton exchange membrane (~130 μm). The anode and cathode catalyst inks were prepared by dispersing the CN@PtRu/CNTs and the Pt/C in isopropanol/water=5/2 (v/v) and 5 wt.% Nafion ionomer. After ultrasonication treatment for 60 min, the obtained anode and cathode catalyst inks were spread by a spray gun onto a carbon paper (3 × 4 cm, HCP135). The MEA was obtained by hot-pressing the anode and cathode carbon papers onto respective sides of Nation 115. at 25 °C and 2.5 MPa for 10 min. A 1.0 M methanol solution was supplied to the anode compartment at a flow rate of 2.0 mL min^{-1}, while the pure oxygen was delivered through the cathode channels at 20 mL min^{-1}. The performance of the DMFCs were evaluated at 80°C. For each experiment, at least three polarization curves were recorded.

1.7. DFT calculations

The DFT calculations with dipole-corrections were performed uisng the Vienna ab-initio simulation package (VASP).[1] The electron‑electron exchange correlations were described using the generalized gradient approximation (GGA) in the form of the Perdew-Burke-Ernzerhof (PBE).[2] The electron-ion interactions were modeled using the projector augment wave (PAW) type pseudopotentials.[3] The cut-off energy was 450 eV for plane-wave expansion. The convergence criteria for energy and force were 1×10^{-5} eV and 0.02 eV $Å^{-1}$, respectively. The Γ-centered k-point mesh was employed to sample the Brillouin zone for both the cell and slab optimization. Specifically, the k-points were chosen to ensure that $a_n \times k_n$ (n = 1, 2, 3) exeeds 30 Å (a_n is the lattice parameters of the cell and slab). Calculations of the MOR energetics were conducted on the (111) surface of the cubic structure of PtRu. The van der Waals corrections were modeled using the DFT-D2 method.[4] A vacuum slab of > 16 Å in z-direction was added to prevent the interactions between the periodic images. Elementary steps of the MOR were simulated using the following reactions:

$$*+CH_3OH \rightarrow CH_3O*+H^+ + e^- \quad \text{(S2)}$$

$$CH_3O* \rightarrow CH_2O*+H^+ + e^- \quad \text{(S3)}$$

$$CH_2O* \rightarrow CHO*+H^+ + e^- \quad \text{(S4)}$$

$$CHO* \rightarrow CO*+H^+ + e^- \quad \text{(S5)}$$

$$CO*+H_2O \rightarrow HO*+CO*+H^+ + e^- \quad \text{(S6)}$$

$$HO*+CO* \rightarrow HOCO* \quad \text{(S7)}$$

$$HOCO* \rightarrow *+CO_2+H^+ + e^- \quad \text{(S8)}$$

where * represents a active site of the catalyst. The Gibbs free energy change (ΔG) of each elementary step was calculated using:

$$\Delta G = \Delta E + \Delta ZPE - T\Delta S \quad \text{(S9)}$$

where ΔE is the calculated binding energy change of the intermediates, ΔZPE and ΔS represent the zero-point and entropy changes of each step.

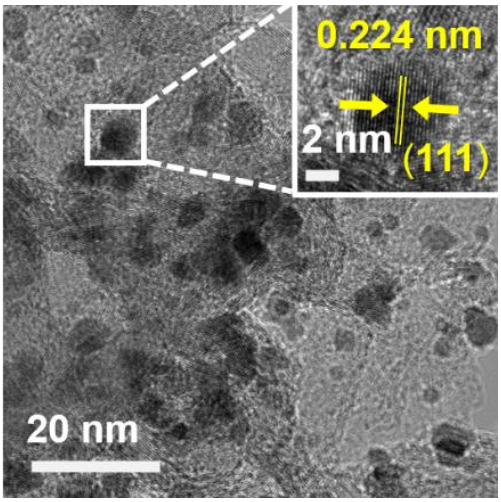

Figure S1. HRTEM image of CN@Pt/CNTs.

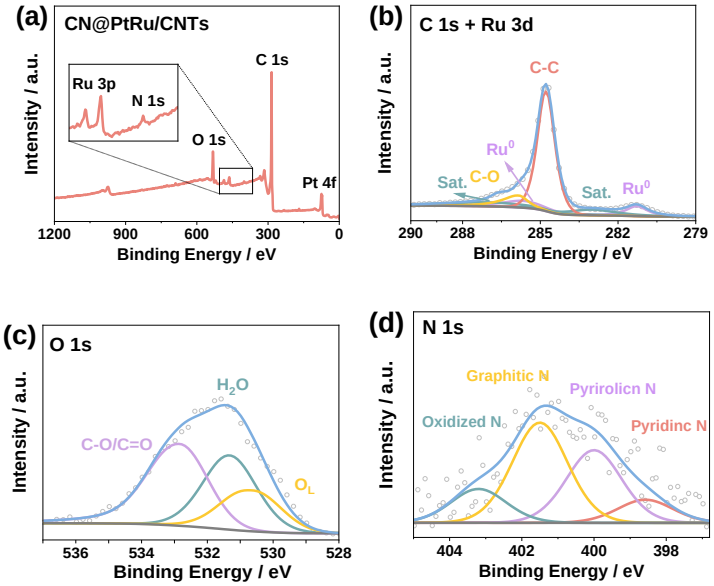

Figure S2. (a) XPS survey spectrum, (b) C 1s + Ru 3d, (c) O 1s, and (d) N 1s of CN@PtRu/CNTs.

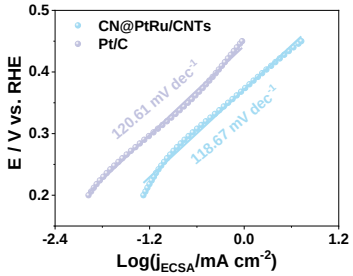

Figure S3. Tafel slope of CN@PtRu/CNTs and Pt/C.

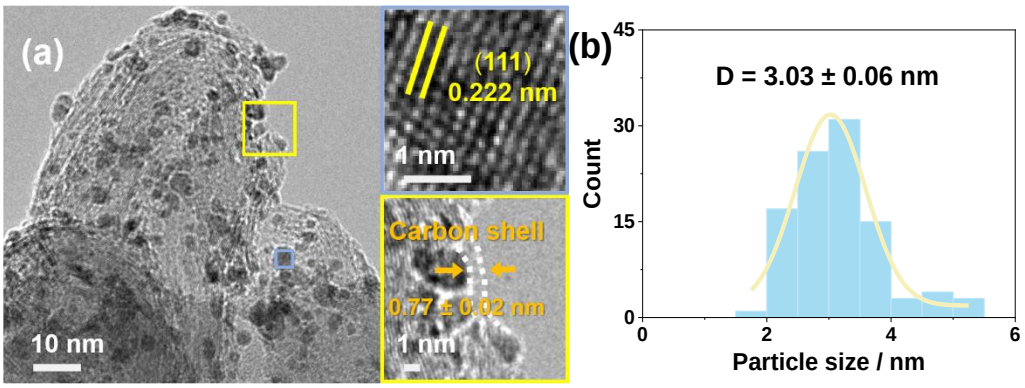

Figure S4. HRTEM image of the CN@PtRu/CNTs after the MOR. The right panel shows the lattice fringes (upper) and the magnified HRTEM (lower) of the PtRu NPs, respectively. (b) Particle size distribution histogram of the PtRu NPs in CN@PtRu/CNTs after the MOR.

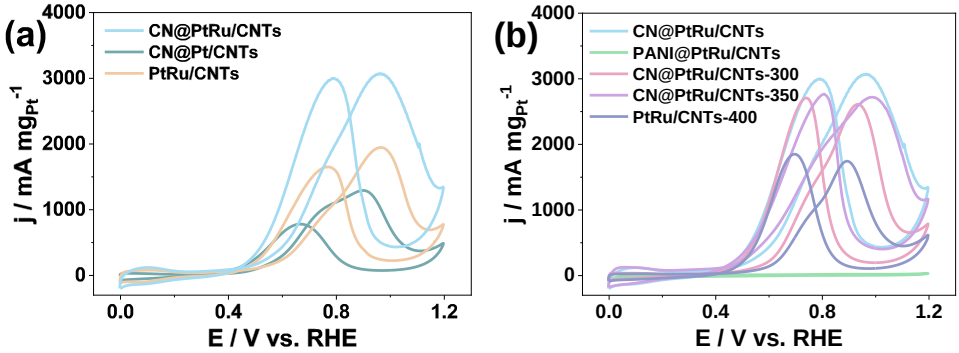

Figure S5. (a) CV curves of CN@PtRu/CNTs, CN@Pt/CNTs and PtRu/CNTs. (b) CV curves of CN@PtRu/CNTs, PANI@PtRu/CNTs, CN@PtRu/CNTs-300, CN@PtRu/CNTs-350 and PtRu/CNTs-400.

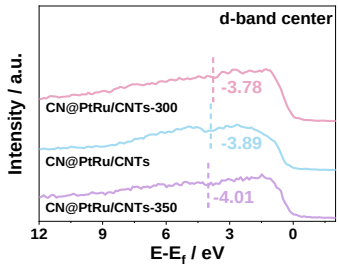

Figure S6. Valence band spectra (VBS) of CN@PtRu/CNTs-300, CN@PtRu/CNTs and CN@PtRu/CNTs-350 with the d-band centers indicated.

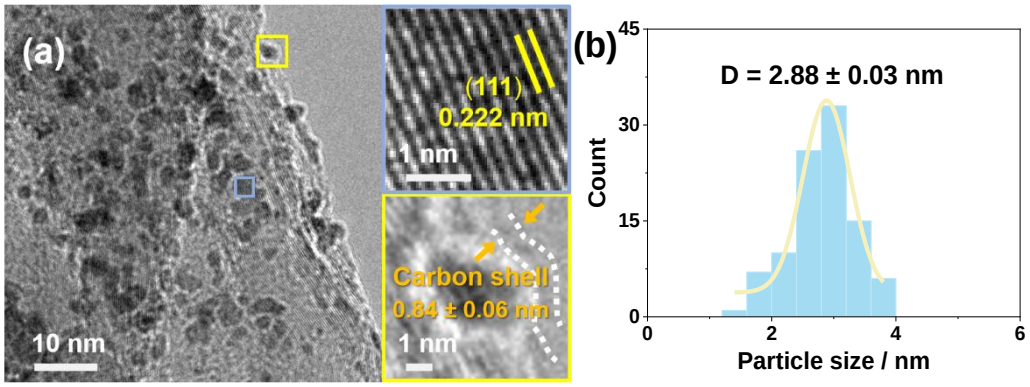

Figure S7. HRTEM image of the CN@PtRu/CNTs-300. The right panel shows the lattice fringes (upper) and the magnified HRTEM (lower) of the PtRu NPs, respectively. (b) Particle size distribution histogram of the PtRu NPs in the CN@PtRu/CNTs-300.

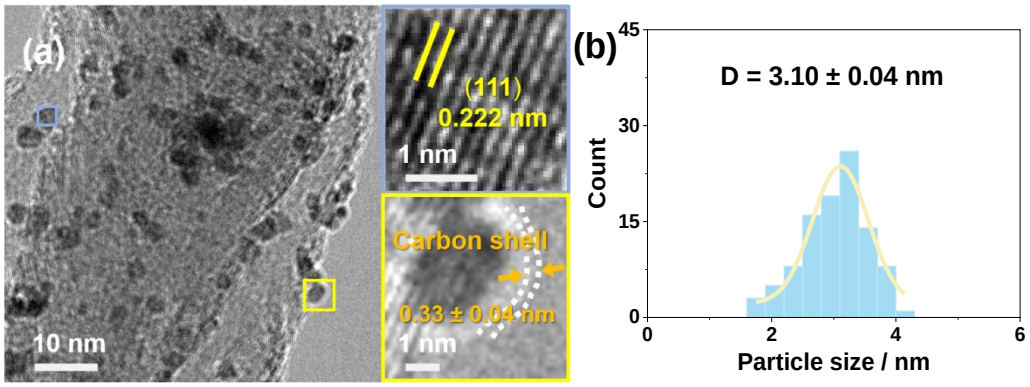

Figure S8. HRTEM image of the CN@PtRu/CNTs-350. The right panel shows the lattice fringes (upper) and the magnified HRTEM (lower) of the PtRu NPs, respectively. (b) Particle size distribution histogram of the PtRu NPs in the CN@PtRu/CNTs-350.

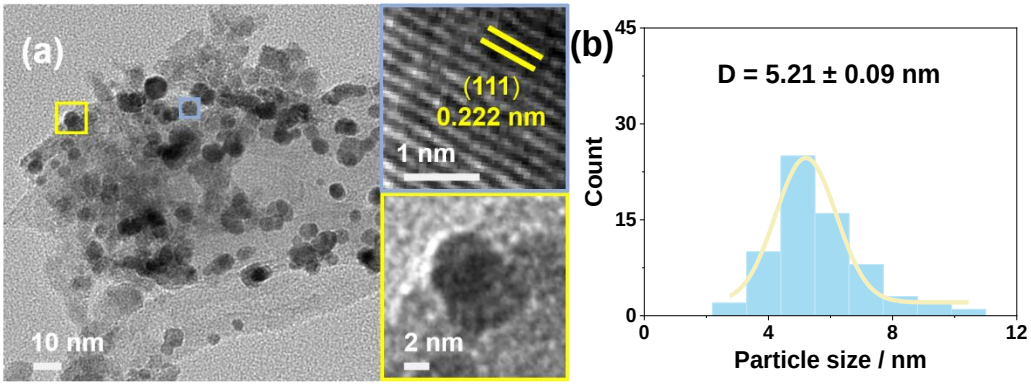

Figure S9. HRTEM image of the PtRu/CNTs-400. The right panel shows the lattice fringes (upper) and the magnified HRTEM (lower) of the PtRu NPs, respectively. (b) Particle size distribution histogram of the PtRu NPs in the PtRu/CNTs-400.

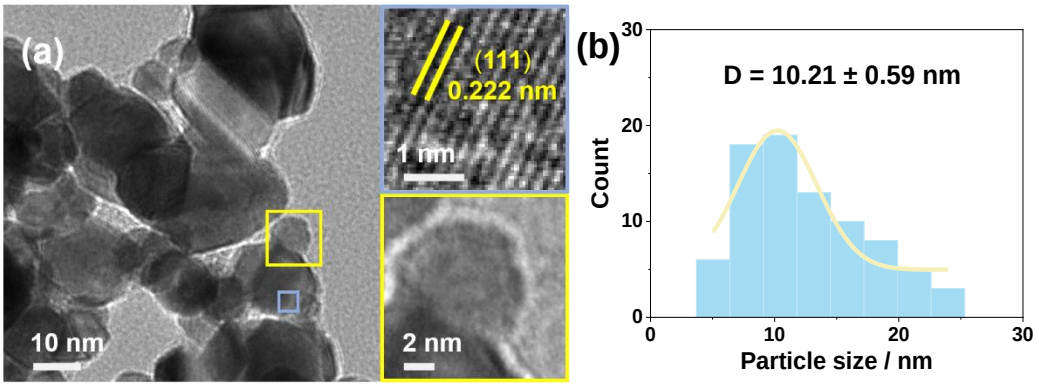

Figure S10. HRTEM image of the PtRu-500. The right panel shows the lattice fringes (upper) and the magnified HRTEM (lower) of the PtRu NPs, respectively. (b) Particle size distribution histogram of the PtRu NPs in the PtRu-500.

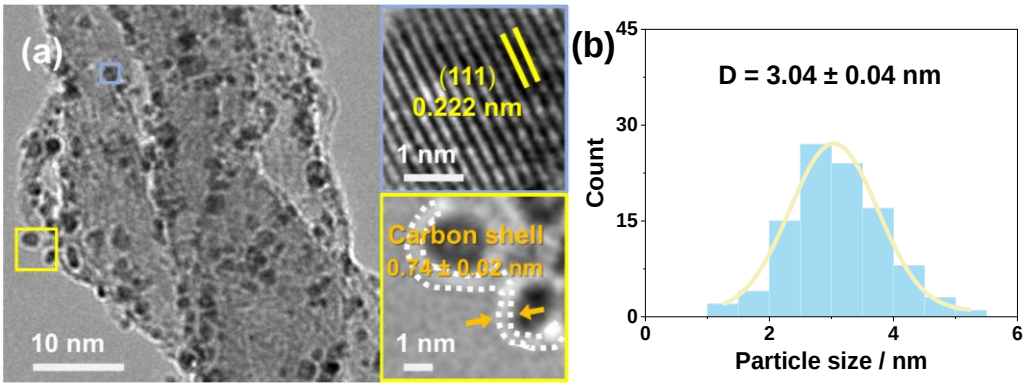

Figure S11. HRTEM image of the CN@PtRu/CNTs after the DMFCs operation. The right panel shows the lattice fringes (upper) and the magnified HRTEM (lower) of the PtRu NPs, respectively. (b) Particle size distribution histogram of the PtRu NPs in CN@PtRu/CNTs after the DMFCs operation.

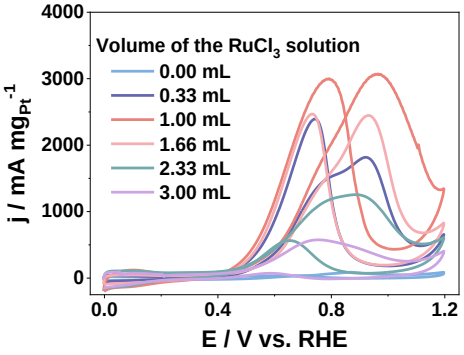

Figure S12. Optimization of Pt/Ru atomic ratio for the MOR catalytic activity. MOR activity screening of CN@PtRu/CNTs synthesized by fixing the volume of H_2PtCl_6 solution (1.0 mL, 0.03 mmol mL^{-1}) and adjusting the volume of $RuCl_3$ solution (0.03 mmol mL^{-1}). The result indicates that the catalyst fabricated with equal volumes of the two precursor solutions delivers the optimal MOR activity, and with its actual Pt-to-Ru atomic ratio verified to be 1.74:1.00.

Table S1. MOR performance comparison of CN@PtRu/CNTs with those reported.

Catalyst	**Mass activity (mA mg_{Pt}^{-1})**	**Tafel slope (mV dec^{-1})**	**Stability**	**Peak power density (mW cm^{-2})**	**Ref.**
CN@PtRu/CNTs	3072.85	118.67	10 h	94.03	This work
PtRu/C($NaBH_4$)	530.00	183.00	1 h	81.8	5
PtRu(2:1)MNs/C	111.77	-	1 h	-	6
Pt@C/NrGO7-OCNTs3	1508.00	-	3 h	-	7
PtFe@PtRuFe	690.00	-	3000 s	-	8
Pt_1Ru_1/NiFe-LDHs-CB	2031.00	-	1 h	-	9
PtRu/TiO_2/ONCNT-400	511.60	-	500 cycles	-	10
PtRu-CVDG	280.30	-	-	-	11
$Pt_{2.7}Ru_{0.3}Sc$ alloy	1030.00	-	-	-	12
PtRu NWs	820.00	-	400 s	-	13
Pt_2Ru_1 alloy NWs	1290.00	-	8000 s	-	14
PtRu/PC-H	1674.20	-	2 h	83.7	15
PtRu/Ti_3C_2Tx	449.00	146	-	3.43	16
PtRu/C	195.40	-	4000 cycles	-	17
Fe-PtRu	1170.00	143	2000 cycles	-	18

References

1. G. Kresse and J. Furthmüller, *Phys. Rev. B.*, 1996, **54**, 11169.
2. J. P. Perdew, K. Burke and M. Ernzerhof, *Phys. Rev. Lett.*, 1996, **77**, 3865.
3. S. Goedecker, M. Teter and J. Hutter, *Phys. Rev. B*, 1996, **54**, 1703.
4. S. Grimme, *J. Comput. Chem.*, 2006, **27**, 1787-1799.
5. Q. Wang, Y.-W. Zhou, Z. Jin, C. Chen, H. Li and W.-B. Cai, *Catalysts*, 2021, **11**, 925.
6. J. Guo, Q. Yan, M. Zhang, J. Fang, S. Luo and J. Xu, *Nanoscale Adv.*, 2024, **6**, 5106-5111.
7. Y. Yu, T. Wang, K. Chen, Q. Wu, Y. Zhang, D. Shi and H. Li, *J. Power Sources*, 2025, **632**, 236395.
8. Q. Wang, S. Chen, P. Li, S. Ibraheem, J. Li, J. Deng and Z. Wei, *Appl. Catal. B: Environ.*, 2019, **252**, 120-127.
9. L. Jin, Q. Meng, M. Ma, X. Gao, A. Chen, X. Sun and D. Zhou, *Green Chem.*, 2024, **26**, 3221-3228.
10. A. Sekar, N. Metzger, S. Rajendran, A. Elangovan, Y. Cao, F. Peng, X. Li and J. Li, *ACS Appl. Nano Mater.*, 2022, **5**, 3275-3288.
11. Z. Tao, W. Chen, J. Yang, X. Wang, Z. Tan, J. Ye, Y. Chen and Y. Zhu, *Sci. China Mater.*, 2019, **62**, 273-282.
12. C. Sun, Y. Liu, Z. Liang, Q. Li, Y. Du, J.-C. Liu, Y. Cheng and F. Luo, *Catal. Sci. Technol.*, 2025, **15**, 2473-2481.
13. L. Huang, X. Zhang, Q. Wang, Y. Han, Y. Fang and S. Dong, *J. Am. Chem. Soc.*, 2018, **140**, 1142-1147.
14. K. Wang, T. Zhou, J. He, Z. Cao and Z. Jiang, *Mol. Catal.*, 2024, **556**, 113927.
15. J. Zhang, X. Qu, Y. Han, L. Shen, S. Yin, G. Li, Y. Jiang and S. Sun, *Appl. Catal. B: Environ.*, 2020, **263**, 118345.
16. N. Abdullah, S. Rahman, A. M. Zainoodin and N. Aslfattahi, *J. Electroanal. Chem.*, 2022, **925**, 116884.
17. G. Xu, *Ionics*, 2018, **24**, 3915-3921.
18. J. Chen, M. Xiao, J. Wan, X. Zheng, C. Li, C. Deng, P. Zhao, M. Ran, Z. Mao and Y. Nie, *J. Alloys Compd.*, 2026, 188017.